



Think Before You Move: Latent Motion Reasoning for Text-to-Motion Generation

Yijie Qian, Juncheng Wang, Yuxiang Feng, Chao Xu, Wang Lu, Yang Liu, Baigui Sun, Yiqiang Chen, *Fellow, IEEE*, Yong Liu, *Member, IEEE*, Shujun Wang, *Member, IEEE*

Abstract—Current state-of-the-art paradigms predominantly treat Text-to-Motion (T2M) generation as a direct translation problem, mapping symbolic language directly to continuous poses. While effective for simple actions, this “System 1” approach faces a fundamental theoretical bottleneck we identify as the **Semantic-Kinematic Impedance Mismatch**: the inherent difficulty of grounding semantically dense, discrete linguistic intent into kinematically dense, high-frequency motion data in a single shot. In this paper, we argue that the solution lies in an architectural shift towards **Latent System 2 Reasoning**. Drawing inspiration from Hierarchical Motor Control in cognitive science, we propose Latent Motion Reasoning (LMR) that reformulates generation as a two-stage “Think-then-Act” decision process. Central to LMR is a novel **Dual-Granularity Tokenizer** that disentangles motion into two distinct manifolds: a compressed, semantically rich Reasoning Latent for planning global topology, and a high-frequency Execution Latent for preserving physical fidelity. By forcing the model to autoregressively “reason” (plan the coarse trajectory) before it “moves” (instantiates the frames), we effectively bridge the ineffability gap between language and physics. We demonstrate LMR’s versatility by implementing it for two representative baselines: T2M-GPT (discrete) and MotionStreamer (continuous). Extensive experiments show that LMR yields non-trivial improvements in both semantic alignment and physical plausibility, validating that the optimal substrate for motion planning is not natural language, but a learned, motion-aligned concept space. Codes and demos can be found in <https://chenhaoqcdyq.github.io/LMR/>.

Index Terms—Text-to-Motion, Reasoning Generative Model, Latent Reasoning Model, Autoregressive Model.

arXiv:2512.24100v1 [cs.CV] 30 Dec 2025

1 INTRODUCTION

The rapid evolution of generative models has transformed Text-to-Motion (T2M) generation [1], [2], [3], [4], [5] from a niche subfield into a critical frontier for computer animation and embodied AI. Current state-of-the-art paradigms predominantly treat T2M as a direct translation problem: a sequence-to-sequence mapping where a source modality (natural language) is projected directly onto a target modality (joint rotations or positions) [6], [7]. While “System 1” [13] approaches (Fig. 1-(a),(b)) achieve success in simple tasks via reflexive feed-forward mapping, they are constrained by the **Semantic-Kinematic Impedance Mismatch**, which hinders the accurate modeling of physically nuanced dynamics [14], [15], [16].

Corresponding to: Yong Liu, Shujun Wang; Yijie Qian and Juncheng Wang contribute equally in this project.

Yijie Qian, Yuxiang Feng, Yong Liu are with Zhejiang University, Hangzhou, China. Email: yijieqian@zju.edu.cn, fengyx1026@gmail.com, yongliu@iipc.zju.edu.cn.

Juncheng Wang, Shujun Wang are with the Hong Kong Polytechnic University, Hong Kong, China. Email: wjc2830@gmail.com, shujun.wang@polyu.edu.hk.

Chao Xu, and Baigui Sun are with IROOTECH TECHNOLOGY and Wolf 1069 b Lab, Sany Group, Hangzhou, China. Email: chaoxuxc@gmail.com, sunbaigui85@gmail.com.

Yang Liu is with IROOTECH TECHNOLOGY; King’s College London, London, United Kingdom and Wolf 1069 b Lab, Sany Group, Hangzhou, China. Email: yang.15.liu@kcl.ac.uk

Wang Lu, and Yiqiang Chen are with Institute of Computing Technology, Chinese Academy of Sciences, Beijing, China. Email: newlw230630@gmail.com, yqchen@ict.ac.cn.

This impedance mismatch stems fundamentally from discrepancy between the natural language and raw motion data. The former is discrete, symbolic, and semantically dense [17]; it captures high-level intent (“walk dejectedly”) but discards the low-level, high-frequency continuous information required for execution (velocity profiles, center-of-mass shifts, foot contact timing). Conversely, the latter is continuous, real-valued, and kinematically dense but semantically sparse. Bridging this gap with a single neural network requires inferring precise physical dynamics directly from abstract linguistic descriptors, necessitating the simultaneous resolution of two orthogonal optimization objectives: semantic alignment and physical control [18], [19]. The result is often “gliding,” physical implausibility, or generic motion that lacks the nuanced style implied by the text.

We argue that the solution lies not in advanced tokenization representations or generative paradigms, but in a fundamental architectural shift towards **Latent System 2 Reasoning** [13], [20], [21]. In cognitive science and motor neuroscience, biological systems do not map high-level goals directly to muscle activations [22], [23], [24]. Instead, biological agents adopt a **Hierarchical Motor Control** strategy that synthesizes a “Generalized Motor Program” (GMP) [25], [26], [27] to serve as an abstract latent representation of movement intent, which is subsequently modulated into specific neuromuscular execution commands. This intermediate stage acts as a cognitive buffer, a “reasoning space” where the system resolves ambiguity and plans the trajectory topology before committing to physical

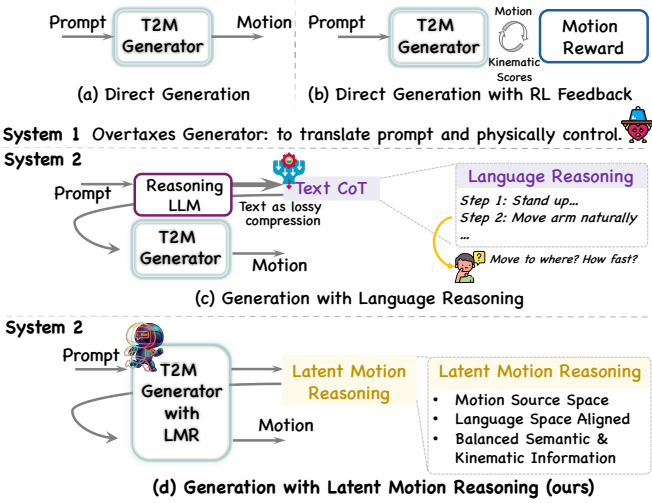


Fig. 1. Architectural Comparison and the Central Challenge of Text-to-Motion (T2M) Generation. Existing methods struggle to bridge the gap between abstract language and continuous motion. (a) **Direct Generation** [8], [9] and (b) **Direct Generation with Feedback** [10], [11] (collectively, System 1) are severely limited by the **Semantic-Kinematic Impediment**, where the generator must simultaneously plan global trajectory and guarantee local physical fidelity, resulting in a single-shot, over-burdened process and outputs that lack physical grounding. (c) **The Language CoT Paradigm** [12] introduces high-level reasoning (System 2), but the textual chain-of-thought is a Low-Bandwidth Bottleneck (Funnel), losing the high-frequency information necessary for realistic dynamics—a limitation known as the **Ineffability of Language**. (d) **Our Latent Motion Reasoning (LMR)** overcomes these limitations by operating entirely within the Dual-Granularity Latent Space. This “Think-then-Act” architectural shift disentangles planning from execution, allowing the model to **autoregressively** reason over a compressed trajectory before instantiating the **physically plausible** motion, effectively harmonizing semantic intent with kinematic demands.

execution. Inspired by this, Chain of Thought (CoT) [28] and Latent Reasoning [29] have sparked revolutionary advances in Large Language Models (LLMs).

Consequently, we propose that T2M generation requires a similar architectural evolution: the introduction of an intermediate reasoning phase. However, we argue that a direct adaptation relying on **explicit language reasoning** (Fig. 1-(c)), such as the textual intermediate steps employed by Motion-R1 [12], is inherently ill-suited for the continuous nature of motion tasks [30]. This limitation stems from the **inherent ineffability** of physical dynamics. While natural language excels at semantic abstraction, it acts as a lossy compression algorithm for kinematics; describing the precise transition of weight or the subtle damping of a joint during a dance move is verbose and imprecise in English, yet geometrically distinct in a high-dimensional vector space. Therefore, restricting the reasoning process to the linguistic domain forces the model to discard essential high-frequency signal, limiting its planning capabilities to **language fluency** while failing to ensure **physical validity**.

In this paper, we posit that the optimal substrate for this planning phase is not natural language, but a latent modality (Fig 1-(d)). By introducing an intermediate latent reasoning stage— $p(\text{latent}|\text{text})$ —we allow the model to engage with a rich, intermediate abstraction that captures the physics and style of the motion before expanding it

into raw frames via $p(\text{motion}|\text{latent})$. This paradigm shifts T2M from a task of translation to one of **progressive instantiation**, bridging the ineffability gap by allowing the model to think in motion-aligned concepts before it acts.

This shift prompts a critical inquiry: **what constitutes an effective latent substrate that balances semantic tractability with physical fidelity?** To answer this, our research commences with empirical studies probing the nature of the feature spaces of motion token sequences. Firstly, we analyze the manifolds induced by different pre-training objectives. We observe a distinct orthogonality: latent spaces optimized for semantic alignment efficiently capture global temporal structure (the *what* and *why*), while those optimized for reconstruction capture local geometric precision (the *how*). This reveals that *learning objective of tokenizers are determining the capacity of semantic or kinematic knowledge* (“knowledge capacity”). Secondly, we re-examine the established trade-off in tokenization. While conventional wisdom suggests that longer token sequences degrade generation due to accumulation error, our empirical observations reveal a more nuanced reality: the bottleneck is not sequence length per se, but the compression rate. Low-compression tokenizers achieves better reconstruction performance by yielding “kinematically dense” tokens, while worse generation performance because those tokens are “semantically sparse”. And vice versa for high-compression tokenizers. Hence, *the compression rate of tokenzier is determining how the semantic or kinematic knowledge distributed over tokens* (“knowledge density”).

Guided by these insights, we instantiate **Latent Motion Reasoning** (LMR), a framework that reformulates autoregressive T2M generation from a flat sequence modeling task into a **hierarchical decision process**. At its core, LMR abandons the monolithic latent assumption in favor of a **Dual-Granularity Tokenization** strategy. We explicitly disentangle the representation into two manifolds: a **Reasoning Latent** and an **Execution Latent**. Specifically, the **Reasoning Latent** is fed with raw motion data (to promise kinematic capacity), and aligned with semantically rich textual embeddings (to promise semantic capacity). And it is further projected through tailored compression rate to modulate the balanced density between kinematic and semantic knowledge. As for the **Execution Latent**, it is optimized purely for reconstruction to preserve high-frequency motion fidelity, to capture the motion’s “dynamics”. Consequently, we restructure the generation horizon into a causal chain: $\text{text} \rightarrow \text{reasoning (plan)} \rightarrow \text{execution (act)}$. By training the generator to predict this structured sequence, LMR forces the model to first hallucinate the coarse-grained topology of the movement before “filling in” the precise physical details. This effectively decouples motion planning from motion instantiation, allowing the model to “think” in stable concepts before committing to volatile frames. With this core, our method can be incorporated with both discrete and continuous style tokenizations.

To demonstrate the versatility of LMR, we implement it at two representative autoregressive T2M baselines: T2M-GPT[3] (discrete token space, cross-entropy loss) and MotionStreamer[9] (continuous token space, diffusion loss). Extensive experiments across three benchmarks demonstrate substantial improvements over these backbones,

specifically achieving a 71% and 64% reduction in FID on the HumanML3D [31] and KIT-ML [32] datasets for T2M-GPT, respectively, along with a 15% improvement over MotionStreamer on HumanML3D.

Our contributions are four-fold:

- **Concept:** We identify the Semantic-Kinematic Impedance Mismatch in T2M and propose Latent System 2 Reasoning as a solution, arguing that motion planning is inherently non-linguistic.
- **Analysis:** We reveal two properties in motion tokenization, empirically demonstrating the knowledge capacity and density between semantic alignment (reasoning) and kinematic fidelity (execution) in token sequences.
- **Method:** We propose LMR, a latent reasoning framework utilizing a dual-granularity tokenizer that decouples motion planning from motion execution.
- **Performance:** We demonstrate that LMR significantly boosts the performance of existing state-of-the-art models (T2M-GPT and MotionStreamer), validating the efficacy of the “think before you move” paradigm.

2 RELATED WORKS

2.1 Text-to-Motion Generation

The field of text-to-motion generation has evolved from early deterministic approaches to probabilistic generative frameworks. Early efforts [33], [34], [35], [1] employed GANs [36] and VAEs [37], while others explored joint embedding spaces for better language grounding [38], [39]. However, these methods often struggled with the diversity and quality of long-term motion.

Diffusion-based Methods. With the success of diffusion models in image synthesis, methods like MDM [2] and MotionDiffuse [40] introduced diffusion processes to raw motion sequences. MotionCLIP [41] demonstrated the efficacy of aligning motion with CLIP space. MLD [4] improved efficiency by performing diffusion in a learned latent space. Subsequent works have focused on specific challenges: MotionLCM [5] optimizes runtime efficiency; ReMoDiffuse [42] enhances diversity; DiffCollage [43] enables long-term generation via parallel diffusion; HumanTOMATO [44] focuses on whole-body motion alignment; Fg-T2M [45] targets fine-grained semantic alignment; and MARDM [46] revisits diffusion by integrating it with masked autoregression to reduce representation redundancy.

Discrete Token-based Methods. Another prominent paradigm involves discretizing motion into codebook indices, typically following two architectural branches:

- **Masked Modeling (BERT-style):** Methods like MoMask [47] and MMM [48] employ bidirectional transformers to reconstruct masked tokens. While effective, they typically require ground-truth motion length as a prior. To mitigate this, the concurrent BAMM [49] proposes a hybrid attention masking strategy to unify bidirectional context with autoregressive length prediction.

- **Autoregressive Modeling (GPT-style):** These methods predict tokens sequentially. T2M-GPT [3] established the baseline using VQ-VAE and standard GPT. Recent advancements focus on scalability and streaming. AttT2M [50] enhances semantic alignment via multi-perspective attention. MotionStreamer [9] enables streaming generation through causal constraints. MOGO [51] introduces a hierarchical causal transformer for infinite-length generation. Similarly, MoSa [52] proposes scalable autoregressive modeling with multi-scale token supervision to improve efficiency.

Despite these advancements, a fundamental theoretical bottleneck persists: the **Semantic-Kinematic Impedance Mismatch**. Current state-of-the-art paradigms predominantly treat T2M as a “System 1” direct translation task, attempting to map discrete, symbolic linguistic intent onto kinematically dense, high-frequency pose data in a single pass. While effective for reflexive actions, this approach struggles to resolve the simultaneous objectives of high-level semantic alignment and low-level physical control. Unlike prior works that aggressively downsample motion to mitigate modeling complexity—often at the cost of physical fidelity—we argue that the solution lies in an architectural decoupling. Our LMR framework reformulates generation as a hierarchical “Think-then-Act” process, introducing a latent reasoning buffer that allows the model to bridge the ineffability gap through structured planning before committing to kinematic execution.

2.2 Motion Tokenizer

The quality of motion generation is fundamentally bounded by the tokenizer’s ability to compress and reconstruct dynamics. **Standard VQ-VAE approaches** [53], [3] map motion snippets to single codebook indices but often suffer from “codebook collapse” or loss of fine details. **Residual Quantization (RVQ)** has been adopted by MoMask [47] and MOGO [51] to reduce quantization error by using multiple codebooks sequentially. **Structure-aware approaches** like ParCo [54] decompose motion into body parts to learn distinct codebooks. Recently, **Hierarchical designs** have emerged: MoSa [52] utilizes a multi-scale token preservation strategy to balance global structure and local detail. Besides, due to the lossy compression of quantization based tokenizers, motionstreamer [9] conducts next-token-prediction in continuous space with diffusively predicting a latent by KL-VAE [37].

In summary, the efficacy of motion generation is intrinsically bounded by the tokenizer’s ability to preserve the delicate balance between semantic tractability and kinematic precision. We identify that conventional monolithic tokenizers often fall into two extremes: “Semantic Sparsity”, where high-frequency details dilute the planning signal, or “Kinematic Loss”, where excessive compression discards the nuanced dynamics required for realism. Our approach moves beyond simple temporal downsampling. By implementing a Dual-Granularity Tokenizer, we explicitly disentangle the latent space into two manifolds: a Reasoning Latent optimized for global topology and an Execution Latent reserved for physical fidelity. This design ensures

a robust, motion-aligned foundation for the subsequent reasoning module, effectively addressing the representation gap inherent in existing methods.

2.3 Evolution of Chain-of-Thought: From Linguistic to Latent Reasoning

The paradigm of Chain-of-Thought (CoT) prompting has revolutionized Large Language Models (LLMs) by decomposing complex problems into intermediate, interpretable reasoning steps [55]. This cognitive “System 2” shift has rapidly transcended natural language, expanding into multimodal domains to address challenges in spatial control and structural synthesis. In the visual domain, frameworks such as Visual CoT [56], [57] and VCTP [58], [59] mimic human deduction through iterative inspection. Similarly, layout-based reasoning [60], [61], [62], [63] and the “Thinking with Images” paradigm [64], [65] utilize intermediate symbolic layouts or low-fidelity drafts to facilitate pixel synthesis. Beyond vision, CoT has been employed in music [66], [67] and audio generation [68], [69], [70] to impose high-level structural logic upon low-level waveforms.

However, a fundamental discrepancy remains in how reasoning is grounded when transitioning from static semantics to dynamic physics. In the specific context of motion generation, recent attempts like Motion-R1 [12] and CoT-Pose [71] have introduced CoT by decomposing prompts into explicit text-based sub-steps (e.g., planning “stance” before “movement”). While these approaches enhance interpretability, we argue they are ultimately constrained by the *Ineffability of Language*. Natural language, being discrete and symbolic, acts as a lossy, low-bandwidth bottleneck that discards the high-frequency kinematic details—such as velocity profiles and momentum shifts—essential for realistic execution [64], [65].

Our proposed **Latent Motion Reasoning (LMR)** represents a pivotal departure from these linguistic-centric paradigms. Instead of forcing physical dynamics into the narrow confines of text, LMR implements CoT reasoning within a motion-aligned latent space. By operating in this dual-granularity manifold, the model can “think” using high-dimensional concepts that are semantically dense yet kinematically grounded. This shift effectively bridges the Semantic-Kinematic Impedance Mismatch: rather than a mere translation of symbols, T2M generation becomes a process of progressive instantiation, where the model resolves global trajectory topology in the reasoning latent before committing to volatile physical frames.

3 PRELIMINARIES OF TEXT-TO-MOTION GENERATION

In this section, we formulate the text-to-motion (T2M) task and review the standard autoregressive frameworks that serve as the backbone for our proposed method.

3.1 Problem Formulation

Let $\mathbf{x} = [x_1, x_2, \dots, x_{T_m}]$ represent a sequence of motion frames, where each $x_t \in \mathbb{R}^d$ describes the pose (e.g., joint rotations and root trajectory) at time step t . Given a natural language description c , the goal of T2M generation is to

model the conditional distribution $p(\mathbf{x}|c)$. To leverage the semantic knowledge of large-scale language models, the text prompt c is typically encoded into a static embedding using a pre-trained encoder such as CLIP [72].

3.2 Motion Tokenization

Due to the high dimensionality and redundancy of raw motion data, state-of-the-art approaches typically compress \mathbf{x} into a lower-dimensional latent sequence before generation. This is achieved via an Encoder-Decoder architecture $(\mathcal{E}, \mathcal{D})$.

3.2.1 Discrete Quantization (VQ-VAE)

In discrete frameworks (e.g., T2M-GPT), the motion is mapped to a sequence of codebook indices. The encoder \mathcal{E} maps \mathbf{x} to latent features $f \in \mathbb{R}^{T' \times d'}$, which are then discretized using a learnable codebook $\mathcal{Z} = \{z_k\}_{k=1}^K$. The quantization operation replaces each feature vector with its nearest codebook neighbor:

$$q = \arg \min_k \|f - z_k\|_2 \quad (1)$$

3.2.2 Continuous Representation (VAE)

In continuous frameworks (e.g., MotionStreamer), vector quantization is omitted to preserve arithmetic properties of the latent space. Instead, a Variational Autoencoder (VAE) is often used, where the encoder predicts parameters of a distribution (e.g., μ, σ) from which the latent tokens are sampled. This effectively projects the motion onto a continuous manifold bounded by a regularization term, such as KL-divergence.

3.3 Standard Autoregressive Modeling

Standard autoregressive (AR) models decompose the generation of the motion sequence S into a product of conditional probabilities:

$$p(S|c) = \prod_{t=1}^{T'} p(S_t|S_{<t}, c) \quad (2)$$

A Transformer backbone \mathcal{H}_θ processes the text condition c and the history of generated tokens $S_{<t}$ to produce a hidden state $h_t = \mathcal{H}_\theta(S_{<t}, c)$ at each time step t . The modeling of the distribution $p(S_t|\cdot)$ depends on the nature of the latent space:

3.3.1 Discrete Autoregression (Classification)

In discrete approaches (e.g., T2M-GPT), S_t is a codebook index. The hidden state h_t is projected via a linear head to a categorical distribution, and the model is trained via Cross-Entropy loss to predict the next token index.

3.3.2 Continuous Autoregression (AR-Diffusion)

In continuous approaches (e.g., MotionStreamer), $S_t \in \mathbb{R}^{d'}$ is a continuous vector. Rather than regressing S_t directly (which often leads to mean-collapse), the distribution $p(S_t|S_{<t}, c)$ is modeled by a conditional diffusion process. At each temporal step t , the AR hidden state h_t serves as the condition for a denoising network ϵ_ϕ . The token S_t is

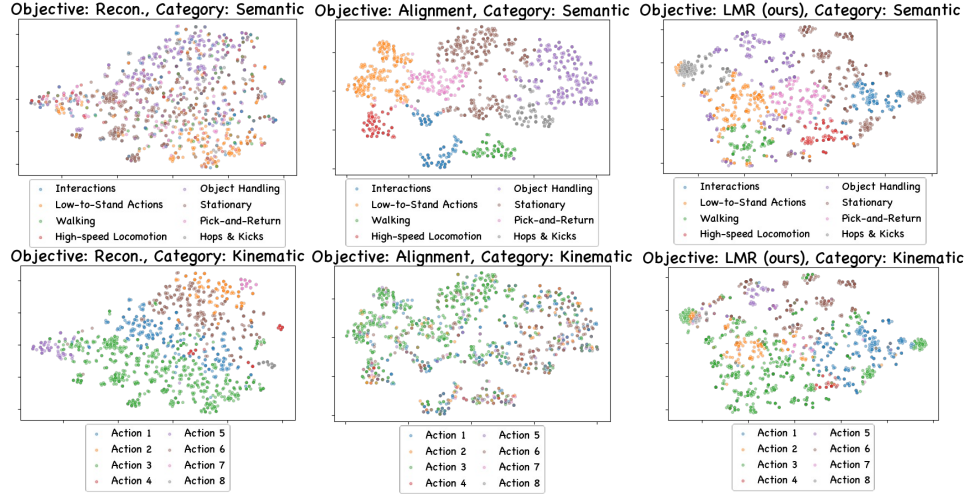


Fig. 2. **Visualization of the Manifold Orthogonality between Semantic Alignment and Kinematic Fidelity.** We employ t-SNE to project motion representations learned under three distinct objectives: **(Left) Reconstruction-only** (\mathcal{L}_{rec}), **(Middle) Alignment-only** (\mathcal{L}_{align}), and **(Right) Our LMR Framework**. The Top Row colors samples by high-level semantic categories (e.g., Interactions, Object Handling), while the **Bottom Row** colors them by specific kinematic sequences, which is ineffability, thus denoted as Action X. **Observation:** A fundamental trade-off is observed in single-objective baselines. The Reconstruction objective yields tight kinematic clusters (Left-Bottom) but results in **semantically entangled manifolds** (Left-Top). Conversely, the Alignment objective creates clear semantic boundaries (Middle-Top) but causes **kinematic blurring** (Middle-Bottom), losing fine-grained physical distinctiveness. **(Right) Our LMR**, via its Dual-Granularity Tokenizer, successfully reconciles this conflict, maintaining clear separability in both semantic intent and kinematic execution spaces.

generated by iteratively denoising a Gaussian noise sample $S_t^{(L)} \sim \mathcal{N}(0, I)$ over L diffusion timesteps:

$$S_t^{(l-1)} = \text{Denoise}(S_t^{(l)}, l, h_t) \quad (3)$$

During training, this is optimized via a Denoising Score Matching objective applied at every sequence position t :

$$\mathcal{L}_{diff} = \mathbb{E}_{t, l, \epsilon} [\| \epsilon - \epsilon_\phi(S_t^{(l)}, l, h_t) \|_2^2] \quad (4)$$

where $S_t^{(l)}$ is the noisy version of the ground truth token at diffusion step l . This paradigm requires running the full diffusion reverse process to instantiate the token at step t before the AR model can proceed to step $t + 1$. Crucially, these standard approaches map semantic intent c directly to kinematic execution S in a single pass, creating the *Semantic-Kinematic Impedance Mismatch* discussed in introduction section.

4 ON THE KNOWLEDGE CAPACITY AND DENSITY IN TOKEN SPACES

To address the *Semantic-Kinematic Impedance Mismatch*, this paper advocates for a “System 2” architectural shift, decomposing generation into high-level planning and low-level execution. However, implementing this paradigm necessitates a specific representational substrate: a latent space that is sufficiently abstract to align with linguistic intent, yet sufficiently grounded to control physical kinematics.

We posit that the optimality of such a substrate is defined by a delicate **Knowledge Balance** between semantic abstraction and kinematic fidelity. To systematically analyze this balance, we formulate two governing properties of motion tokenization:

- **Knowledge Capacity (The Manifold):** This refers to the intrinsic scope of information the latent manifold

is capable of representing. We hypothesize that the *type* of knowledge a tokenizer prioritizes—whether global semantics or local geometry—is fundamentally determined by its **pre-training objectives**.

- **Knowledge Density (The Sequence):** This refers to the concentration of information allocated to each individual token in the autoregressive sequence. We hypothesize that the *richness* of the reasoning signal versus the sparsity of the execution detail is directly dictated by the tokenizer’s **temporal compression rate**.

To validate this framework, we conduct two pilot studies to reveal how the training objectives (Sec. 4.1) and compression rates (Sec. 4.2) serve as the distinct control levers for Capacity and Density, respectively.

4.1 Pre-Training Objectives: The Manifold Orthogonality

To validate how pre-training objectives govern the manifold, we analyze the latent geometries induced by the two dominant pre-training objectives in T2M: *Reconstruction* (\mathcal{L}_{rec}) [37] and *Semantic Alignment* (\mathcal{L}_{align}) [73].

We train two distinct motion tokenizer variants on the HumanML3D dataset. Model A (VQ-VAE) is trained with reconstruction objective \mathcal{L}_{rec} (MSE), while Model B (TMR Encoder [73]) uses a contrastive objective \mathcal{L}_{align} , aligning motion features with CLIP text embeddings. We probe these latent spaces via two distributions. Given the same tokenized motion sequences, we visualize the cluster distributions according to two distinct label sets, one label set classifies sequences according to the semantic meaning (such as “interactions”, “object handling”), while another label distinguishes sequences as the kinematic actions (such as those with similar joint angles).

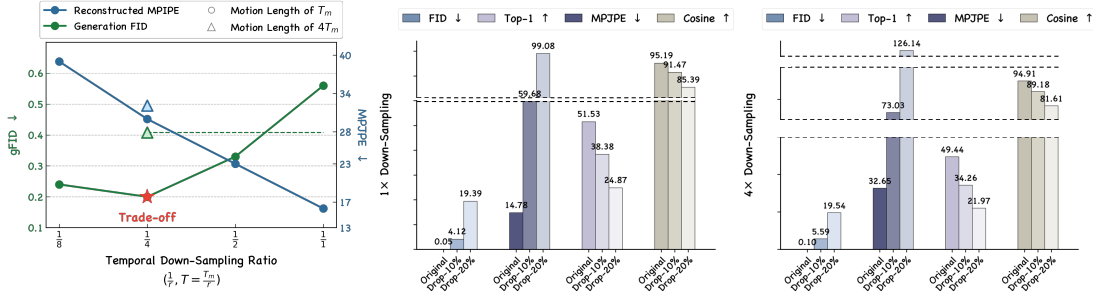


Fig. 3. **Analysis of Semantic Density and Temporal Resolution.** (Left) **The Reconstruction-Generation Trade-off:** We plot reconstruction error (MPJPE, Blue) and generation quality (FID, Green) across varying down-sampling ratios. A clear trade-off is observed: while high-frequency tokens (1/1) yield the best reconstruction, they degrade generation quality. The optimal balance is found at a 1/4 ratio (Red Star). Crucially, the “Same Token Length” comparison (Triangles vs. Circles with a temporal down-sampling ratio of $\frac{1}{4}$) reveals that a long motion sequence compressed by 4× (Hollow Triangle) generates significantly better motion than a short, uncompressed sequence of the same token count ($\frac{1}{4}$ Circles). This confirms that **Semantic Density**, rather than sequence length, is the governing factor for generation quality. (Middle & Right) **Information Sparsity Probe:** We evaluate semantic robustness by testing the retrieval performance using token sequences with randomly dropped tokens. The high-frequency representation (Middle, 1×) exhibits higher redundancy (slower decay in Cosine similarity and Top-1 Accuracy) compared to the compressed representation (Right, 4×). This indicates that semantic information in raw motion is **highly sparse and diluted**, creating a “contextual sprawl” that hinders effective autoregressive modeling.

As visualized in Fig. 2, t-SNE projections reveal a fundamental orthogonality in how these objectives structure the latent space:

- **Semantic Clustering (\mathcal{L}_{align}):** The alignment-optimized space organizes data by intent (as shown by the second column of Fig. 2). Distinct sequences that share a semantic label (e.g., “boxing” punch vs. “boxing” dodge) are drawn together, while sequences with the same action labels seem to be randomly distributed.
- **Kinematic Clustering (\mathcal{L}_{rec}):** The reconstruction-optimized space organizes data by geometric similarity (as shown by the first column of Fig. 2). Motions with similar kinematic dynamics are clustered tightly. However, semantic concepts (e.g., “interactions” vs. “walking”) are entangled.

Takeaway 1: The Necessity of Manifold Disentanglement. These findings confirm our hypothesis regarding **Knowledge Capacity**: we observe a fundamental “Manifold Orthogonality” where latent spaces optimized for kinematic reconstruction (\mathcal{L}_{rec}) and semantic alignment (\mathcal{L}_{align}) evolve into mutually exclusive topologies. This indicates that a monolithic latent space suffers from an inherent capacity bottleneck—it cannot simultaneously accommodate the high-frequency geometric precision required for execution and the abstract semantic clustering required for reasoning. Consequently, the optimal substrate is not a compromise, but a decoupling. This motivates the **Manifold Disentanglement** in our Dual-Granularity Tokenizer (Sec. 5), which assigns distinct subspaces to maximize the capacity for semantic planning (“the what”) and kinematic instantiation (“the how”) independently, and then aggregates the knowledge capacity in a shared encoder.

4.2 Tokenization Temporal Compression Rate

Complementing our analysis of pre-training objectives, we now examine the *temporal resolution* of the latent space. While the learning objective determines *what* features are preserved, the tokenization rate dictates their *distribution*. We identify a fundamental tension: high-frequency tokenizers (with less compression rate) minimize reconstruction error but dilute semantic signals, creating a “contextual sprawl” that hinders autoregressive (AR) modeling. This paradox compels us to investigate the trade-off between physical fidelity and sequence modeling tractability.

4.2.1 Sequence Length Trade-off Analysis

Given a motion sequence with a length of T_m , if we increase the token sequence T , it naturally improves reconstruction but exacerbates long-term dependencies. To probe this, we evaluate VQ-VAE configurations across varying down-sampling rates ($T \in T_m \times \{1, 1/2, 1/4, 1/8\}$). As shown in Fig. 3, we observe a non-monotonic trend: while reconstruction (MPJPE) improves linearly with length, generation quality (gFID) plateaus at $T = T_m/4$. This suggests that simply increasing resolution yields diminishing returns for generation due to modeling complexity.

4.2.2 The Semantic Density Hypothesis

To isolate the impact of temporal resolution, we further utilize two motion sequences, one with a length of T_m , another with $4 \times T_m$ (by up-sampling the same T_m motion). For T_m motion, we utilize a high-frequency tokenizer (no temporal compression). As for $4 \times T_m$ motion, we utilize a relatively low-frequency tokenizer (four times temporal compression). With such, we can derive two motion sequences with the same length.

However, we compare the generation performances over these two token sequences, where we observe that *the longer motion sequence achieves better generation FID, even if reconstructing it is harder*. This confirms that the bottleneck is not sequence length, but **Knowledge Density**—defined as the ratio of information content per token. High-frequency sequences dilute semantic intent across many frames, while

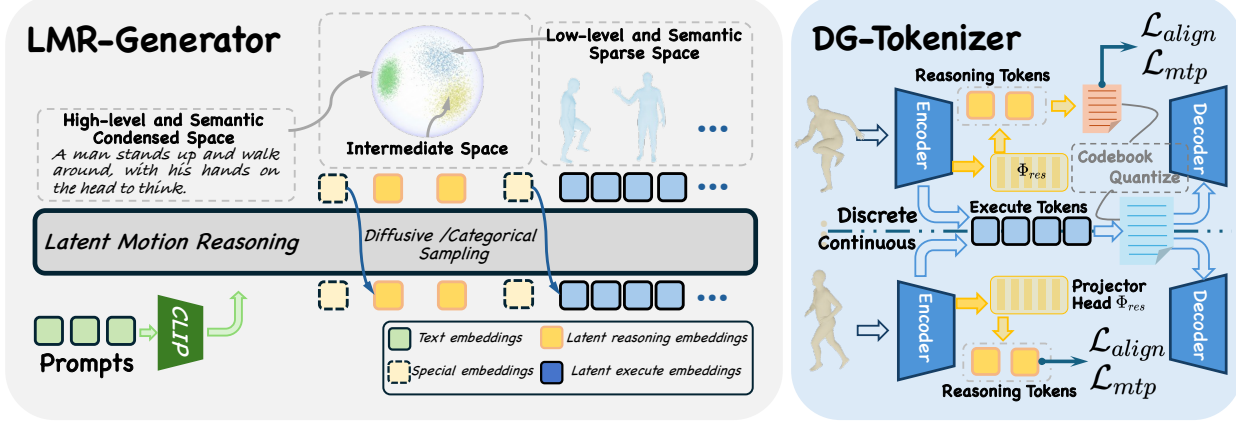


Fig. 4. **Overview of the proposed Latent Motion Reasoning (LMR) framework.** The framework consists of two phases: **(Right) Dual-Granularity (DG) Tokenizer:** We explicitly disentangle motion representations into two manifolds: a compressed Reasoning Latent (Yellow), which is aligned with text embeddings to capture high-level semantic intent, and a high-frequency **Execution Latent** (Blue), which preserves low-level kinematic fidelity for reconstruction. **(Left) LMR-Generator:** We reformulate T2M as a hierarchical “Think-then-Act” generation process. Conditioned on the text prompt, the model first autoregressively synthesizes the coarse-grained reasoning tokens to establish the global motion topology (Thinking Phase). These tokens then serve as a stable semantic condition to guide the subsequent generation of fine-grained execution tokens (Acting Phase) via either Categorical or Diffusive sampling.

preserve more kinematic details. And vice versa for low-frequency sequences. This is further validated by our ablation studies (middle&right columns of Fig. 3): randomly dropping tokens in longer sequences causes significantly lower retrieval degradation than in shorter ones, proving that semantic information is highly redundant and distributed in high-frequency regimes.

Takeaway 2: Bridging the Granularity Gap via Latent Buffering. These findings substantiate the critical role of **Knowledge Density** in autoregressive modeling. We observe that high-frequency tokenization induces a “contextual sprawl” that dilutes semantic intent, resulting in prediction ambiguity within flat autoregressive frameworks. To construct a **Knowledge Balanced** latent reasoning sequence, it is imperative to decouple the temporal resolution of planning from execution. This insight directly motivates the temporal abstraction strategy in our LMR, which enforces a distinct, compressed sequence length for the reasoning phase to maximize knowledge density.

5 LATENT MOTION REASONING

Guided by the analysis in Sec. 4, we introduce **Latent Motion Reasoning (LMR)**. LMR reformulates Text-to-Motion generation as a **Hierarchical Decision Process**. Instead of mapping text directly to motion tokens, we factorize the generation probability into a two-stage causal chain:

$$p(\mathbf{x} | c) \approx \underbrace{p(S_{exec} | S_{res}, c)}_{\text{Execution (System 1)}} \cdot \underbrace{p(S_{res} | c)}_{\text{Reasoning (System 2)}}, \quad (5)$$

where S_{res} is a highly compressed, semantically dense “Reasoning Latent” sequence, and S_{exec} is a high-frequency “Execution Latent” sequence.

5.1 Dual-Granularity Tokenizer

To materialize the proposed hierarchical reasoning, we design a tokenizer that projects raw motion \mathbf{x} into two disentangled manifolds: a **Reasoning Manifold** (low-frequency, semantic-dense) and an **Execution Manifold** (high-frequency, kinematic-dense). The architecture begins with a shared encoder backbone \mathcal{E} that extracts a base feature sequence $\mathbf{f} = \mathcal{E}(\mathbf{x}) \in \mathbb{R}^{T \times d'}$ without temporal compression. From this shared representation, the pipeline bifurcates into two modality-specific implementations.

5.1.1 Scenario A: Discrete Dual-Codebook Quantization

In the discrete setting (e.g., for T2M-GPT [3] baselines), we require the latent space to be categorical. To support the distinct roles of planning and execution, we introduce a **Dual-Codebook** mechanism comprising a Reasoning Codebook \mathcal{Z}_{res} and an Execution Codebook \mathcal{Z}_{exec} .

The Execution Branch (Kinematic VQ): This branch aims to preserve maximal physical detail. We utilize the full-resolution features \mathbf{f} and quantize them using a large, expressive codebook $\mathcal{Z}_{exec} \in \mathbb{R}^{N_{exec} \times d'}$.

$$\mathbf{q}_{exec} = \arg \min_k \|\mathbf{f} - \mathcal{Z}_{exec}^{(k)}\|_2, \quad \hat{\mathbf{f}}_{exec} = \mathcal{Z}_{exec}(\mathbf{q}_{exec}). \quad (6)$$

This yields a sequence \mathbf{q}_{exec} of length T , providing the fine-grained tokens required for precise motion reconstruction.

The Reasoning Branch (Semantic VQ): This branch constructs the “motor plan.” We first apply a projection head Φ_{res} on \mathbf{f} , obtaining \mathbf{f}_{res} . Then, we employ a separate, compact codebook $\mathcal{Z}_{res} \in \mathbb{R}^{N_{res} \times d'}$ to discretize these features:

$$\mathbf{q}_{res} = \arg \min_k \|\mathbf{f}_{res} - \mathcal{Z}_{res}^{(k)}\|_2, \quad \hat{\mathbf{f}}_{res} = \mathcal{Z}_{res}(\mathbf{q}_{res}). \quad (7)$$

The resulting sequence \mathbf{q}_{res} has length $T/4$. Unlike \mathcal{Z}_{exec} which learns local pose geometry, \mathcal{Z}_{res} is trained to act as a dictionary of “motion concepts” or actemes.

5.1.2 Scenario B: Continuous Dual-Projection

In the continuous setting (e.g., for MotionStreamer [9] baselines), quantization is unnecessary. Instead, the focus is on shaping the continuous latent density to be conducive to diffusion processes.

The Execution Branch: We retain the raw continuous output of the encoder, serving as the ground truth for the diffusion model’s reconstruction target:

$$\mathbf{u}_{exec} = \mathbf{f} \in \mathbb{R}^{T \times d'}. \quad (8)$$

We apply a slight KL-regularization penalty $KL(\mathbf{u}_{exec} || \mathcal{N}(0, I))$ to ensure the manifold is bounded, facilitating stable diffusion training.

The Reasoning Branch: Instead of quantization, we apply an auto-encoder. Similar to the discrete case, we downsample the sequence to $T/4$ by the Φ_{res} projection head, obtaining continuous latent tokens \mathbf{u}_{res} , which serve as the clean condition for the diffusion process.

5.1.3 Training Objectives for Semantic Density

Regardless of the modality (Discrete or Continuous), the **Reasoning Branch** must be forced to capture semantics rather than just compressed kinematics. We impose two auxiliary losses specifically on the reasoning features ($\hat{\mathbf{f}}_{res}$ or \mathbf{u}_{res}):

Semantic Alignment (BERT Loss): To inject language awareness, we maximize the cosine similarity between the pooled reasoning features $\hat{\mathbf{f}}_{res}/\mathbf{u}_{res}$ and the BERT [74] embedding of the text prompt \mathbf{w} :

$$\mathcal{L}_{align} = 1 - \cos(\text{AvgPool}(\mathbf{u}_{res}), \mathbf{w}), \quad (9)$$

where we use \mathbf{u}_{res} as a demonstration, and likewise below.

Masked Text Prediction (MTP): To ensure fine-grained semantic density, we train a lightweight decoder to reconstruct masked words in the text prompt solely from the reasoning tokens:

$$\mathcal{L}_{mtp} = \text{CrossEntropy}(\text{Decoder}(\mathbf{u}_{res}), \mathbf{w}_{masked}), \quad (10)$$

where \mathbf{w}_{masked} denotes the masked language sequence.

The total tokenizer loss is a weighted sum of the reconstruction loss (on the execution branch), the VQ/KL regularization terms, and these semantic objectives.

$$\mathcal{L} = \mathcal{L}_{rec} + \lambda_{align} * \mathcal{L}_{align} + \lambda_{mtp} * \mathcal{L}_{mtp} + \mathcal{L}_{VQ/KL}. \quad (11)$$

This ensures that \mathbf{u}_{res} (or $\hat{\mathbf{f}}_{res}$) emerges as a valid substrate for System 2 reasoning.

5.2 Generative Process: Unified Autoregressive Modeling

A key advantage of LMR is its architectural flexibility: it integrates seamlessly into existing autoregressive backbones by adopting the native representation space of the host model. Whether the backbone operates on discrete codebook indices (e.g., T2M-GPT) or continuous latent vectors (e.g., MotionStreamer), LMR unifies planning and execution into a **single heterogeneous sequence**.

We define the generation target as a concatenated sequence $[\mathbf{u}_{res}; \mathbf{u}_{exec}]$ (continuous) or $[\mathbf{q}_{res}; \mathbf{q}_{exec}]$ (discrete). A single Transformer backbone \mathcal{H}_θ models the joint probability autoregressively. We detail the realization of this unified process in two distinct modalities:

5.2.1 Scenario A: Discrete Token Space (e.g., T2M-GPT)

In this setting, both the reasoning and execution manifolds are discretized via Vector Quantization [75]. The reasoning tokens \mathbf{q}_{res} correspond to indices from the LMR Codebook \mathcal{Z}_{res} , while \mathbf{q}_{exec} corresponds to indices from the Execution Codebook \mathcal{Z}_{exec} .

The Transformer \mathcal{H}_θ operates as a standard causal language model. At each step t , it predicts the categorical distribution of the next token. We employ a **Switching Prediction Head** strategy:

$$p(S_t | S_{<t}, c) = \begin{cases} \sigma(\mathbf{W}_{res}^T \cdot h_t) & \text{if } t \leq T/4 \text{ (Reasoning Phase)} \\ \sigma(\mathbf{W}_{exec}^T \cdot h_t) & \text{if } t > T/4 \text{ (Execution Phase)} \end{cases} \quad (12)$$

where $h_t = \mathcal{H}_\theta(S_{<t}, c)$ is the hidden state, σ is the softmax. Crucially, during the execution phase ($t > T/4$), the self-attention mechanism has full visibility of the completed reasoning sequence \mathbf{q}_{res} . This allows the model to attend back to the “motor plan” to guide the synthesis of precise motion details, effectively solving the long-horizon forgetting problem via a compact semantic prefix.

5.2.2 Scenario B: Continuous Feature Space (e.g., MotionStreamer)

In this setting, we bypass vector quantization during generation. Both reasoning and execution tokens remain in the continuous domain. Here, \mathbf{u}_{res} consists of the continuous, and semantic-aligned features, while \mathbf{u}_{exec} consists of the full-resolution motion features.

We adopt the **Autoregressive Diffusion** paradigm. The Transformer \mathcal{H}_θ functions as a conditional denoiser. For each step t in the concatenated sequence, the model synthesizes the continuous vector S_t via a diffusion reverse process. The training objective is a unified Denoising Score Matching loss:

$$\mathcal{L}_{diff} = \mathbb{E}_{t, l, \epsilon} \left[\|\epsilon - \mathcal{H}_\theta(S_t^{(l)}, l, S_{<t}, c)\|_2^2 \right], \quad (13)$$

where l is the diffusion timestep and $S_t^{(l)}$ is the noisy version of the current token.

Unified Reasoning-Execution Transition: Even in this continuous space, the structural advantage remains identical. The model first “denoises” the trajectory of the abstract reasoning vectors. Once the planning steps are complete, it transitions to denoising the execution vectors. Because the backbone is autoregressive, the generation of the high-frequency execution features is conditioned on the noise-free, stable trajectory of the reasoning features generated in the first $T/4$ steps.

5.2.3 Summary of Inference Flow

In both scenarios, inference proceeds as a single “Think-then-Act” stream: 1. **Phase I (Reasoning):** The model autoregressively generates the first $T/4$ tokens. These tokens, being semantically dense and temporally compressed, rapidly establish the global topology of the motion. 2. **Phase II (Execution):** The model continues generating from $t = T/4 + 1$ to T . The high-frequency kinematic dynamics are “filled in” by attending to the semantic constraints established in Phase I.

This formulation demonstrates that LMR is not tied to a specific generative loss (Cross-Entropy vs. Diffusion) but

TABLE 1

Comparison with diffusion-, BERT-, and GPT-type models of text-conditional motion synthesis on the HumanML3D and KIT-ML test set. \pm indicates a 95% confidence interval. Among GPT-type methods, we indicate the best result in **bold** face, and the second best in underline.

Datasets	Methods	R Precision↑			FID↓	MultiModal Dist↓	Diversity →
		Top 1	Top 2	Top 3			
Human ML3D	Ground Truth	0.511 \pm .003	0.703 \pm .003	0.797 \pm .002	0.002 \pm .000	2.974 \pm .008	9.503 \pm .065
	MDM [2]	-	-	0.611 \pm .007	0.544 \pm .044	5.566 \pm .027	9.559 \pm .086
	MLD [4]	0.481 \pm .003	0.673 \pm .003	0.772 \pm .002	0.473 \pm .013	3.196 \pm .010	9.724 \pm .082
	MotionDiffuse [40]	0.491 \pm .001	0.681 \pm .001	0.782 \pm .001	0.630 \pm .001	3.113 \pm .001	9.410 \pm .049
	MMM [48]	0.504 \pm .003	0.696 \pm .003	0.794 \pm .004	0.080 \pm .004	2.998 \pm .007	9.411 \pm .058
	MoMask [47]	0.521 \pm .002	0.713 \pm .002	0.807 \pm .002	<u>0.045</u> \pm .002	2.958 \pm .008	-
	BAMM [49]	0.525 \pm .002	0.720 \pm .003	0.814 \pm .003	0.055 \pm .002	2.919 \pm .008	9.717 \pm .089
	MotionGPT [76]	0.492 \pm .003	0.681 \pm .003	0.778 \pm .002	0.232 \pm .008	3.096 \pm .009	9.528 \pm .071
	ParCo [54]	0.515 \pm .003	0.706 \pm .003	0.801 \pm .002	0.109 \pm .005	2.927 \pm .008	<u>9.576</u> \pm .088
	Mogo [51]	0.505 \pm .003	0.693 \pm .003	0.799 \pm .003	0.079 \pm .002	3.002 \pm .008	-
KIT- ML	T2M-GPT [3]	0.492 \pm .003	0.679 \pm .002	0.775 \pm .002	0.141 \pm .005	3.121 \pm .009	9.761 \pm .151
	LMR(Ours)	0.537 \pm .005	0.721 \pm .004	<u>0.810</u> \pm .005	0.040 \pm .002	2.895 \pm .017	9.668 \pm .077
	Ground Truth	0.424 \pm .005	0.649 \pm .006	0.779 \pm .006	0.031 \pm .004	2.788 \pm .012	11.080 \pm .097
	MDM [2]	-	-	0.396 \pm .004	0.497 \pm .021	9.191 \pm .022	10.847 \pm .109
	MLD [4]	0.390 \pm .008	0.609 \pm .008	0.734 \pm .007	0.404 \pm .027	3.204 \pm .027	10.80 \pm .117
	MotionDiffuse [40]	0.417 \pm .004	0.621 \pm .004	0.739 \pm .004	1.954 \pm .062	2.958 \pm .005	11.10 \pm .143
	MMM [48]	0.381 \pm .005	0.590 \pm .006	0.718 \pm .005	0.429 \pm .019	3.146 \pm .019	10.633 \pm .097
	MoMask [47]	0.433 \pm .007	0.656 \pm .005	0.781 \pm .005	0.204 \pm .011	2.779 \pm .022	-
	BAMM [49]	<u>0.438</u> \pm .009	0.661 \pm .009	0.788 \pm .005	<u>0.183</u> \pm .013	2.723 \pm .026	<u>11.008</u> \pm .094
	MotionGPT [76]	0.366 \pm .005	0.558 \pm .004	0.680 \pm .005	0.510 \pm .004	3.527 \pm .021	10.35 \pm .084
KIT- ML	ParCo [54]	0.430 \pm .004	0.649 \pm .007	0.772 \pm .008	0.453 \pm .027	2.820 \pm .028	10.95 \pm .094
	Mogo [51]	0.420 \pm .007	0.634 \pm .007	0.754 \pm .007	0.313 \pm .016	2.957 \pm .029	-
	T2M-GPT [3]	0.416 \pm .006	0.627 \pm .006	0.745 \pm .006	0.514 \pm .029	3.007 \pm .023	10.921 \pm .108
	LMR(Ours)	0.483 \pm .012	0.701 \pm .007	<u>0.811</u> \pm .006	0.181 \pm .006	2.636 \pm .014	11.032 \pm .128

is rather a universal strategy for **Hierarchical Temporal Modeling**.

6 EXPERIMENT

6.1 Experimental Setup

Datasets. We evaluate our method on two standard motion-language benchmarks: HumanML3D [31] and KIT-ML [32]. The HumanML3D dataset comprises 14,616 motions sourced from AMASS [77] and HumanAct12 [78], with each motion annotated by three text descriptions, totaling 44,970 descriptions. The KIT-ML dataset provides a smaller-scale evaluation platform with 3,911 motions and 6,278 text descriptions. All motion sequences are split into training (80%), testing (15%), and validation (5%) sets.

Metrics. We adhere to the standard evaluation protocol proposed in T2M [8]. We employ Frechet Inception Distance, denoted as **FID**, to measure the distributional divergence between synthesized and ground-truth motion sequences. We evaluate semantic consistency via **R-Precision** at Top-1, Top-2, and Top-3 levels and Multimodal Distance, or **MM-Dist**. We assess generation variety using **Diversity**, which measures the variance in generated motions. For execution evaluation, we utilize Mean Per Joint Position Error, **MPJPE**. For reasoning evaluation, we measure the prediction accuracy, **ACC**, of masked keywords in the input descriptions, acting as a proxy for local semantic alignment.

Implementation Details. We implement our framework in PyTorch and train on NVIDIA H200 GPUs. We instantiate LMR with two backbones to validate its generality.

Discrete Setting. We adopt the 263-dimensional joint position representation [31] and VQ-VAE architecture from [3] with codebook size 512. The execution encoder is first

trained with batch size 256 and learning rate $2e-4$. We then freeze it and train the reasoning branch for 200K iterations with $\lambda_{align} = 0.5$ and $\lambda_{mtp} = 0.1$. The generator follows T2M-GPT with 18 Transformer layers and 1024 hidden dimensions, trained for 300K iterations with batch size 256. During inference, we apply Classifier-Free Guidance with scale $s = 2.0$.

Continuous Setting. We employ the 272-dimensional SMPL rotation representation [9], which bypasses Inverse Kinematics post-processing. The execution branch adopts a Causal Temporal AutoEncoder. After training the execution branch for 2M iterations, we freeze it and train the reasoning branch for 200K iterations with learning rate $1e-4$ and identical loss weights with $\lambda_{align} = 0.5$, $\lambda_{mtp} = 0.1$. The generator comprises a 12-layer Transformer (768 hidden dim), incorporated with a 9-layer MLP diffusion head. Training proceeds for 300K iterations with batch size 256 and cosine learning rate schedule (peak $1e-4$). During inference, we set the guidance scale $s = 5.0$.

Reasoning Branch Architecture. The reasoning branch operates on the encoded motion representations from the execution branch encoder. Specifically, it employs a 2-layer causal Transformer with 4 attention heads and 512 hidden dimensions, with a feed-forward dimension of 1024, followed by a 4x temporal downsampling module. For the discrete setting, a vector quantizer with codebook size 512 discretizes these features into reasoning tokens. For the continuous setting, a VAE encoder maps the features into a 16-dimensional latent space.

Masked Token Prediction. For \mathcal{L}_{mtp} , we employ a frozen BERT-base model with structured masking targeting action verbs, body parts, directional modifiers, and their compositions. The reasoning tokens are fed into a 2-layer cross-

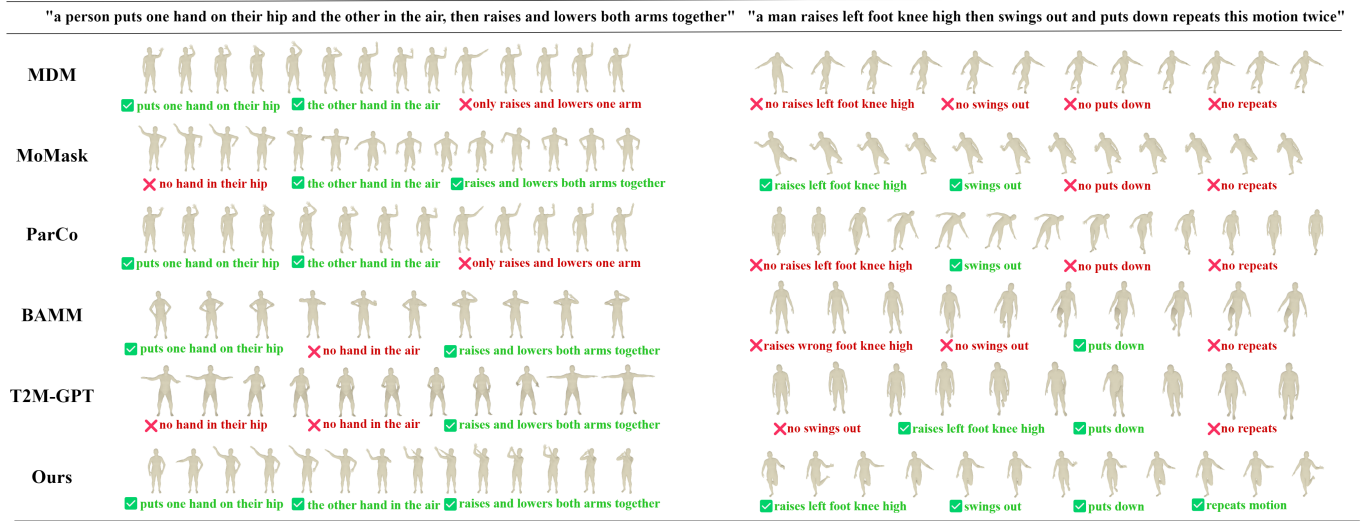


Fig. 5. Qualitative comparison with state-of-the-art methods under the discrete motion representation setting.

TABLE 2

Quantitative comparison on HumanML3D test set under the **continuous motion representation setting** [9]. Real motion serves as an upper-bound reference. Lower FID and MultiModal Dist are better; higher R-Precision and Diversity are better. Among *generated* methods, **bold** denotes best, underline denotes second best.

Methods	R Precision↑			FID↓	MultiModal Dist↓	Diversity→
	Top 1	Top 2	Top 3			
Real motion	0.702	0.864	0.914	0.002	15.151	27.492
T2M-GPT [3]	0.606	0.774	0.838	12.475	16.812	27.275
MotionGPT [76]	0.456	0.598	0.628	14.375	17.892	27.114
MoMask [47]	0.621	0.784	0.846	12.232	16.138	27.127
AttT2M [50]	0.592	0.765	0.834	15.428	15.726	26.674
MotionStreamer [9]	0.631	<u>0.802</u>	0.859	<u>11.790</u>	16.081	<u>27.284</u>
LMR(Ours)	0.644	0.812	0.869	<u>9.937</u>	<u>15.968</u>	27.373

attention Transformer decoder with 4 heads, 768 hidden dimensions, and 1536 feed-forward dimensions to predict masked text tokens, encouraging fine-grained semantic learning. Dropout is applied during training.

6.2 Comparison with State-of-the-Arts

Quantitative Results. Table 1 and Table 2 present a comprehensive comparison against state-of-the-art Diffusion, GPT, BERT, and Hybrid frameworks. Our analysis yields three key observations regarding the efficacy of Latent Motion Reasoning (LMR):

Architectural Decoupling vs. Component Engineering (Table 1). On the discrete benchmark, LMR significantly outperforms its backbone T2M-GPT (FID 0.141→**0.040** on HumanML3D) and advanced GPT variants like Mogo [51] and ParCo [54]. This indicates that the semantic bottleneck in autoregressive modeling is fundamental; it requires explicitly decoupling reasoning from execution rather than merely scaling codebook capacity or decomposing body parts.

Planning vs. Correction (Table 1). Compared to BERT-based masked models (MMM, MoMask), LMR achieves superior diversity and semantic alignment without relying on ground-truth motion length—a critical limitation in MoMask. Furthermore, LMR outperforms BAMM, a hybrid method that generates then refines. This validates our core

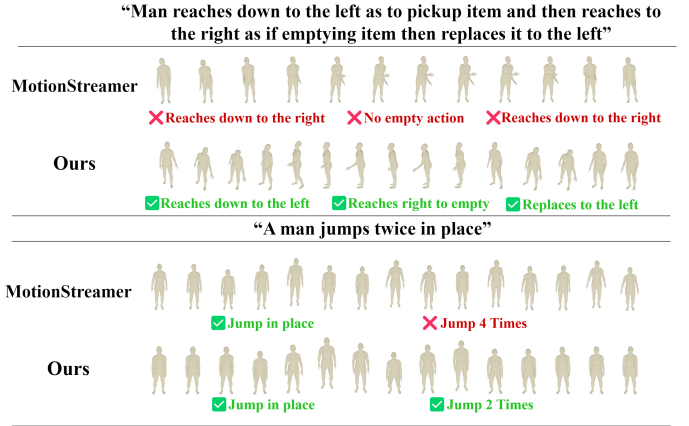


Fig. 6. Qualitative comparison with MotionStreamer [9] under the continuous motion representation setting.

hypothesis: planning the topology before execution (“Think-then-Act”) is a more effective inductive bias than generating followed by post-hoc correction.

Generalizability and Representation Sensitivity (Table 2). LMR proves agnostic to the underlying representation. In the continuous setting, it improves the MotionStreamer [9] backbone to achieve the lowest FID of **9.937**. Notably, the performance leap is more pronounced in the discrete domain than the continuous one. We attribute this to the nature of the baselines: discrete quantization creates severe “Semantic Sparsity,” where LMR acts as a critical structural stabilizer. In contrast, continuous diffusion models already benefit from smoothing; here, LMR serves primarily to sharpen semantic alignment rather than rescue the model from structural collapse.

Qualitative Results. Visualizations in Figure 5 and Figure 6 highlight the critical advantage of our hierarchical generation process.

Complex Semantic Reasoning (Figure 5). While standard baselines (T2M-GPT, ParCo) suffer from semantic incompleteness—often ignoring concurrent actions—and hybrid

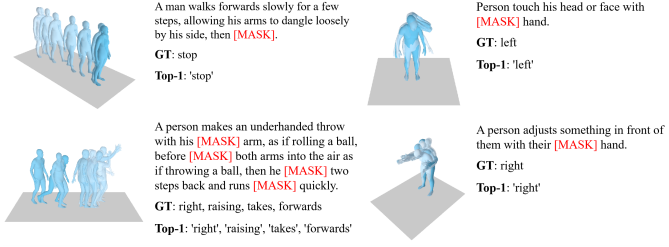


Fig. 7. Visualization of the Masked Token Prediction (MTP) capability. The model predicts masked keywords (marked in red) such as body parts ('left', 'right') and actions ('stop', 'raising') using the learned Reasoning Latents. The high accuracy of Top-1 predictions demonstrates that our reasoning module effectively captures fine-grained semantic-kinematic alignment.

methods (BAMM) struggle with attribute binding (e.g., confusing left/right limbs), LMR accurately resolves strict spatial and compositional constraints. By establishing a global motion topology first, it prevents the structural degradation observed in single-stage models.

Logic-Driven Constraints (Figure 6). In continuous latent spaces, LMR successfully enforces logic-driven requirements such as repetition counting and directional changes, whereas MotionStreamer frequently drifts, failing to maintain the causal logic of the prompt.

Latent Interpretability (Figure 7). Finally, we validate the semantic density of our reasoning tokens via Masked Token Prediction. The model's ability to recover masked keywords solely from the reasoning latent proves that this manifold captures high-level *semantic intent* rather than mere kinematic compression, effectively bridging the linguistic-physical gap.

User Study. Please refer to the Appendix A for more details.

TABLE 3

Ablation study of different token configurations. Exec. and Reas. denote the token sequence length ratio (T/T_m). The Joint setting implies a single sequence handling both tasks.

Method	Token Scale	Execution Quality		Reasoning Alignment		Generation			
		Exec.	Reas.	rFID↓	MPJPE↓	R1↑	ACC↑	gFID↓	MM-Dist↓
Baseline	1/4	—	0.095	30.294	—	—	0.137	3.225	
	1	—	0.044	16.608	—	—	0.242	3.148	
	1 (Joint)	0.083	22.512	0.429	0.463	0.354	3.253		
Ours	1	1/2	0.044	16.608	0.466	0.536	0.212	3.250	
	1	1/4	0.044	16.608	0.474	0.538	0.040	2.895	
	1	1/8	0.044	16.608	0.462	0.533	0.062	3.145	
	1/2	1/8	0.094	24.790	0.468	0.526	0.069	3.182	
	1/2	1/16	0.094	24.790	0.455	0.519	0.076	2.969	
	1/4	1/16	0.095	30.294	0.463	0.533	0.105	3.092	

6.3 Ablation Study

The following ablation studies are conducted on the discrete T2M-GPT backbone with the HumanML3D dataset. In addition to the below experiments, Cross-backbone analyses and Impact of Classifier-Free Guidance involving both discrete and continuous settings are provided in the Appendix A.

6.3.1 Impact of Dual-Granularity Tokenizer (Table 3).

We investigate how execution and reasoning token scales affect reconstruction, semantic alignment, and generation.

For execution tokens, higher resolution yields better reconstruction: 1× achieves MPJPE of 16.608 (row 1), while 1/4× degrades to 30.294 (row 2). However, directly generating high-resolution motion is challenging—note that the 1/4× model attains a significantly better gFID than 1×. This trend is further corroborated by rows 4, 7, and 9. Moreover, since reconstruction quality upper-bounds generation performance, we opt not to downsample the execution tokens. For reasoning tokens, fixing execution at 1× and varying reasoning scale reveals that 1/4× is optimal with gFID of 0.040, as 1/2× lacks sufficient abstraction and 1/8× loses temporal granularity. Additionally, the Joint baseline using a single 1× sequence fails at both reconstruction and generation due to conflicting objectives, while our Dual strategy achieves optimal balance by decoupling execution and reasoning manifolds.

TABLE 4

Ablation study on the training strategies for the dual-branch tokenizer. End-to-End denotes joint training; Two-Stage implies training the execution branch first, followed by the reasoning branch (with freezing or fine-tuning); Independent uses two separate networks.

Training Strategy	Execution Quality		Reasoning Alignment		Generation	
	rFID↓	MPJPE↓	R1↑	ACC↑	gFID↓	MM-Dist↓
End-to-End (Joint)	0.133	22.563	0.499	0.519	0.145	3.174
Two-Stage (Freeze)	0.044	16.608	0.474	0.538	0.040	2.895
Two-Stage (Finetune)	0.101	20.276	0.481	0.549	0.109	3.077
Independent Networks	0.044	16.608	0.489	0.556	0.097	3.134

6.3.2 Training Pipeline Analysis (Table 4).

We evaluate four training strategies for our Dual-Granularity Tokenizer.

End-to-End joint training yields suboptimal generation with gFID of 0.145, as conflicting gradients between reconstruction and semantic objectives degrade execution quality to rFID=0.133 and MPJPE=22.563.

Two-Stage Freeze strategy we employed achieves optimal performance with gFID of 0.040 and MM-Dist of 2.895 by first establishing a high-fidelity execution substrate with FID of 0.044 and MPJPE of 16.608, then freezing it during reasoning branch training to prevent representational drift.

Two-Stage Fine-tune degrades execution quality to FID of 0.101 despite marginally higher semantic alignment at ACC=0.549, resulting in inferior generation with gFID=0.109. This confirms the execution space should remain invariant after initialization.

Independent Networks achieve identical reconstruction and the highest semantic alignment with R1=0.489 and ACC=0.556, yet generation degrades to gFID of 0.097. This stems from architectural disconnection: our reasoning tokens derive from execution encoder features, grounding semantic abstractions in the kinematic manifold. Independent encoders create disjoint representation spaces, introducing a semantic-kinematic gap that impairs generation. This validates our design—shared encoder backbone ensures representational coherence while frozen parameters prevent optimization interference.

6.3.3 Effectiveness of Guidance Strategies.

Table 5 validates the necessity of our learned reasoning tokens by comparing them against three alternative guidance

TABLE 5

Ablation study on alternative guidance strategies. All variants adopt the high-resolution execution tokens (1×). We compare five guidance schemes: off-the-shelf TMR embeddings [73], coarse-to-fine autoregressive generation, extended CLIP token sequences [72], explicit language Chain-of-Thought, and our learned reasoning tokens.

Guidance Strategy	FID↓	R-Precision ↑			MM-Dist↓	Div→
		Top-1	Top-2	Top-3		
Baseline (w/o guidance)	0.242	0.497	0.684	0.778	3.148	9.914
+ TMR Embeddings	0.120	0.472	0.666	0.759	3.210	9.965
+ Coarse-to-Fine AR	0.154	0.488	0.679	0.779	3.097	9.692
+ CLIP Token ($L=77$)	0.206	0.523	0.718	0.812	2.963	9.719
+ Explicit Language CoT	0.188	0.511	0.702	0.795	3.021	9.752
+ Reasoning Tokens (Ours)	0.040	0.537	0.721	0.810	2.895	9.668

TABLE 6

Ablation study on the reasoning loss functions. \mathcal{L}_{align} focuses on aligning the reasoning tokens with the global text embedding, while \mathcal{L}_{mtp} enforces fine-grained semantic understanding via masked text prediction. The combination achieves the best balance.

Reasoning Objective	Reasoning Alignment		Generation Quality		FID↓	MM-Dist↓
	R1↑	ACC↑				
\mathcal{L}_{align}	0.482	0.000		0.136	3.189	
\mathcal{L}_{mtp}	0.036	0.534		0.120	3.161	
$\mathcal{L}_{align} + \mathcal{L}_{mtp}$ (Ours)	0.474	0.538		0.040	2.895	

paradigms.

Latent Representation vs. Off-the-Shelf Embeddings. Replacing our reasoning tokens with pre-trained TMR embeddings [73] degrades R-Precision to 0.472. This confirms that generic motion-language embeddings lack the specific semantic discriminability required for generation. Our reasoning tokens, optimized via joint global alignment and local masked prediction, encode significantly richer control signals.

Manifold Disentanglement vs. Temporal Coarsening. A naive Coarse-to-Fine autoregressive baseline (predicting down-sampled tokens first) yields a poor FID of 0.154 due to error accumulation. This comparison isolates the source of our performance: success stems not merely from progressive generation, but from Manifold Disentanglement. Unlike coarse-to-fine approaches that operate entirely within the kinematic space, LMR establishes the trajectory in a separate, semantically aligned manifold before mapping to execution. This prevents the generation of “compressed but empty” kinematics that lack semantic grounding.

Motion-Aligned Reasoning vs. Linguistic Reasoning. Finally, we examine explicit linguistic guidance via full CLIP sequences [72] and Textual Chain-of-Thought (Motion-R1 style [12]). While these methods improve semantic consistency (R-Precision 0.523 and 0.511), their generation quality remains suboptimal (FID 0.206 and 0.188). This validates that fine-grained text can partially improve performance. However, as we previously claimed, symbolic text is too sparse to effectively guide high-frequency motion synthesis, illustrating the ineffability of physical dynamics. Our approach achieves the best balance (FID 0.040, R-Precision 0.537) by conducting reasoning in a learned, motion-aligned latent substrate—effectively bridging the gap between abstract intent and physical execution.

6.3.4 Reasoning Loss Functions (Table 6).

We examine the roles of \mathcal{L}_{align} for global alignment and \mathcal{L}_{mtp} for local alignment. \mathcal{L}_{align} optimizes global R-Precision but neglects local details with an ACC of 0.000. \mathcal{L}_{mtp} captures fine-grained semantics yielding an ACC of 0.534 but loses global coherence. Combining both in our approach provides the most effective synergy, ensuring the generated plan is both globally consistent and locally precise.

TABLE 7

Efficiency evaluation during training and inference. * employs KV caching to speed up autoregressive generation. Tok. and Gen. denote Tokenizer and Generator.

Method	Infer. (ms/frame)		Train. (H)		Size (M)	
	Tok.	Gen.	Tok.	Gen.	Tok.	Gen.
T2M-GPT [3]	1.1	31	15	40	19.44	228.42
ParCo [54]	1.2	5	4	18	6.35	19.44
MoMask [47]	2.8	15	18	4	25.41	166.05
Ours	2.4	30	5	-	24.79	229.62
Ours*	-	0.4	-	-	-	-

6.3.5 Efficiency Comparison (Table 7).

Table 7 compares training and inference efficiency against T2M-GPT, ParCo, and MoMask. Compared to T2M-GPT, our method introduces additional reasoning layers in the tokenizer, resulting in slightly more parameters and higher per-frame latency. However, this overhead yields significantly better generation quality. ParCo and MoMask reduce network capacity to accelerate inference, but ParCo requires six tokenizer components leading to longer training time, while MoMask needs six sequential passes for RVQ decoding. Notably, neither supports KV caching. In contrast, our autoregressive generator enables KV caching [79], reducing inference time to 0.4 ms/frame.

7 CONCLUSION

This work redefines Text-to-Motion generation by identifying and resolving the **Semantic-Kinematic Impedance Mismatch**—the fundamental friction between abstract linguistic intent and continuous physical dynamics. We introduce **Latent Motion Reasoning (LMR)**, a framework that shifts the field from flat sequence-to-sequence translation to a hierarchical “Think-then-Act” paradigm. By decoupling global motion planning from precise kinematic execution via a **Dual-Granularity Tokenizer**, LMR achieves state-of-the-art performance across both discrete and continuous backbones. Crucially, our findings challenge the utility of explicit linguistic reasoning for physical tasks, demonstrating that the optimal substrate for motion planning is not natural language, but a learned, motion-aligned latent space. LMR represents a pivotal step toward **Cognitive Motion Generation**, moving beyond reflex-based synthesis to systems that possess a genuine, hierarchical understanding of physical behavior.

REFERENCES

- [1] C. Guo, S. Zou, X. Zuo, S. Wang, W. Ji, X. Li, and L. Cheng, "Generating diverse and natural 3d human motions from text," in *Proceedings of the IEEE/CVF conference on computer vision and pattern recognition*, 2022, pp. 5152–5161.
- [2] G. Tevet, S. Raab, B. Gordon, Y. Shafir, D. Cohen-Or, and A. H. Bermano, "Human motion diffusion model," *arXiv preprint arXiv:2209.14916*, 2022.
- [3] J. Zhang, Y. Zhang, X. Cun, Y. Zhang, H. Zhao, H. Lu, X. Shen, and Y. Shan, "Generating human motion from textual descriptions with discrete representations," in *Proceedings of the IEEE/CVF conference on computer vision and pattern recognition*, 2023, pp. 14 730–14 740.
- [4] X. Chen, B. Jiang, W. Liu, Z. Huang, B. Fu, T. Chen, and G. Yu, "Executing your commands via motion diffusion in latent space," in *Proceedings of the IEEE/CVF conference on computer vision and pattern recognition*, 2023, pp. 18 000–18 010.
- [5] W. Dai, L.-H. Chen, J. Wang, J. Liu, B. Dai, and Y. Tang, "Motionlcm: Real-time controllable motion generation via latent consistency model," in *European Conference on Computer Vision*. Springer, 2024, pp. 390–408.
- [6] Y. Yuan, J. Song, U. Iqbal, A. Vahdat, and J. Kautz, "Physdiff: Physics-guided human motion diffusion model," in *Proceedings of the IEEE/CVF International Conference on Computer Vision*, 2023, pp. 16 010–16 021.
- [7] R. Dabral, M. H. Mughal, V. Golyanik, and C. Theobalt, "Mofusion: A framework for denoising-diffusion-based motion synthesis," in *Proceedings of the IEEE/CVF Conference on Computer Vision and Pattern Recognition*, 2023, pp. 9760–9770.
- [8] C. Guo, S. Zou, X. Zuo, S. Wang, W. Ji, X. Li, and L. Cheng, "Generating diverse and natural 3d human motions from text," in *Proceedings of the IEEE/CVF conference on computer vision and pattern recognition*, 2022, pp. 5152–5161.
- [9] L. Xiao, S. Lu, H. Pi, K. Fan, L. Pan, Y. Zhou, Z. Feng, X. Zhou, S. Peng, and J. Wang, "Motionstreamer: Streaming motion generation via diffusion-based autoregressive model in causal latent space," *arXiv preprint arXiv:2503.15451*, 2025.
- [10] X. Liu, Y. Mao, W. Zhou, and H. Li, "Motionrl: Align text-to-motion generation to human preferences with multi-reward reinforcement learning," *arXiv preprint arXiv:2410.06513*, 2024.
- [11] J. Yue, Z. Wang, Y. Wang, W. Zeng, J. Wang, X. Xu, Y. Zhang, S. Zheng, Z. Ding, and Z. Lu, "Rl from physical feedback: Aligning large motion models with humanoid control," *arXiv preprint arXiv:2506.12769*, 2025.
- [12] R. Ouyang, H. Li, Z. Zhang, X. Wang, Z. Zhu, G. Huang, and X. Wang, "Motion-r1: Chain-of-thought reasoning and reinforcement learning for human motion generation," *arXiv preprint arXiv:2506.10353*, 2025.
- [13] D. Kahneman, *Thinking, fast and slow*. macmillan, 2011.
- [14] D. Rempe, T. Birdal, A. Hertzmann, J. Yang, S. Sridhar, and L. J. Guibas, "Humor: 3d human motion model for robust pose estimation," in *Proceedings of the IEEE/CVF International Conference on Computer Vision*, 2021, pp. 11 488–11 499.
- [15] Y. Yuan, S.-E. Ugarte, q. Tate, and K. Kitani, "Simpoe: Simulated character control for 3d human pose estimation," in *Proceedings of the IEEE/CVF Conference on Computer Vision and Pattern Recognition*, 2021, pp. 7159–7169.
- [16] W. Pouw, J. de Wit, S. Bögels, M. Rasenberg, B. Milivojevic, and A. Ozyurek, "Semantically related gestures move alike: Towards a distributional semantics of gesture kinematics," in *International Conference on Human-Computer Interaction*. Springer, 2021, pp. 269–287.
- [17] Y. Li, G. Yan, A. Macaluso, M. Ji, X. Zou, and X. Wang, "Integrating lmm planners and 3d skill policies for generalizable manipulation," *arXiv preprint arXiv:2501.18733*, 2025.
- [18] Y. Xie, F. Juefei-Xu, V. Wang, V. M. Patel, and V. N. Boddeti, "Omnicontrol: Control any joint at any time for human motion generation," in *International Conference on Learning Representations*, 2024.
- [19] K. Karunratanakul, K. Preechakul, S. Suwajanakorn, and S. S. Tang, "Gmd: Graph-based motion diffusion," in *European Conference on Computer Vision*, 2024.
- [20] G. Booch, F. Fabiano, L. Horesh, K. Kate, J. Lenchner, N. Linck, A. Loreggia, K. Murgesan, N. Mattei, F. Rossi *et al.*, "Thinking fast and slow in ai," in *Proceedings of the AAAI Conference on Artificial Intelligence*, vol. 35, no. 17, 2021, pp. 15 042–15 046.
- [21] Z.-Z. Li, D. Zhang, M.-L. Zhang, J. Zhang, Z. Liu, Y. Yao, H. Xu, J. Zheng, P.-J. Wang, X. Chen *et al.*, "From system 1 to system 2: A survey of reasoning large language models," *arXiv preprint arXiv:2502.17419*, 2025.
- [22] P. Egan, R. Sinko, P. R. LeDuc, and S. Keten, "The role of mechanics in biological and bio-inspired systems," *Nature communications*, vol. 6, no. 1, p. 7418, 2015.
- [23] M. L. Latash, "Evolution of motor control: from reflexes and motor programs to the equilibrium-point hypothesis," *Journal of human kinetics*, vol. 19, no. 19, p. 3, 2008.
- [24] S. H. Czyż, M. Zvonař, and E. Pretorius, "The development of generalized motor program in constant and variable practice conditions," *Frontiers in psychology*, vol. 10, p. 2760, 2019.
- [25] M. Carter and D. Shapiro, "Control of sequential movements: Evidence for generalized motor programs," *Journal of neurophysiology*, vol. 52, no. 5, pp. 787–796, 1984.
- [26] J. Merel, L. Hasenclever, A. Galashov, A. Ahuja, V. Pham, G. Wayne, Y. W. Teh, and N. Heess, "Neural probabilistic motor primitives for humanoid control," in *International Conference on Learning Representations*, 2019.
- [27] C. Tessler, Y. Kauten, A. Clegg, D. Mun, J. Merel, and D. Soudry, "Calm: Conditional adversarial latent models for directable virtual characters," *ACM Transactions on Graphics (TOG)*, vol. 42, no. 4, pp. 1–13, 2023.
- [28] J. Wei, X. Wang, D. Schuurmans, M. Bosma, F. Xia, E. Chi, Q. V. Le, D. Zhou *et al.*, "Chain-of-thought prompting elicits reasoning in large language models," *Advances in neural information processing systems*, vol. 35, pp. 24 824–24 837, 2022.
- [29] S. Hao, S. Sukhbaatar, D. Su, X. Li, Z. Hu, J. Weston, and Y. Tian, "Training large language models to reason in a continuous latent space," *arXiv preprint arXiv:2412.06769*, 2024.
- [30] Z. Zhao, Z. Wang, and P. Liu, "Chatmotion: Reasoning-centric text-to-motion generation," *arXiv preprint arXiv:2311.04456*, 2023.
- [31] C. Guo, S. Zou, X. Zuo, S. Wang, W. Ji, X. Li, and L. Cheng, "Generating diverse and natural 3d human motions from text," in *Proceedings of the IEEE/CVF conference on computer vision and pattern recognition*, 2022, pp. 5152–5161.
- [32] M. Plappert, C. Mandery, and T. Asfour, "The kit motion-language dataset," *Big data*, vol. 4, no. 4, pp. 236–252, 2016.
- [33] H. Cai, C. Bai, Y.-W. Tai, and C.-K. Tang, "Deep video generation, prediction and completion of human action sequences," in *Proceedings of the European conference on computer vision (ECCV)*, 2018, pp. 366–382.
- [34] Z. Wang, P. Yu, Y. Zhao, R. Zhang, Y. Zhou, J. Yuan, and C. Chen, "Learning diverse stochastic human-action generators by learning smooth latent transitions," in *Proceedings of the AAAI conference on artificial intelligence*, vol. 34, no. 07, 2020, pp. 12 281–12 288.
- [35] M. Petrovich, M. J. Black, and G. Varol, "Action-conditioned 3d human motion synthesis with transformer vae," in *Proceedings of the IEEE/CVF International Conference on Computer Vision*, 2021, pp. 10 985–10 995.
- [36] I. J. Goodfellow, J. Pouget-Abadie, M. Mirza, B. Xu, D. Warde-Farley, S. Ozair, A. Courville, and Y. Bengio, "Generative adversarial nets," *Advances in neural information processing systems*, vol. 27, 2014.
- [37] D. P. Kingma, M. Welling *et al.*, "Auto-encoding variational bayes," 2013.
- [38] C. Ahuja and L.-P. Morency, "Language2pose: Natural language grounded pose forecasting," in *2019 International Conference on 3D Vision (3DV)*. IEEE, 2019, pp. 719–728.
- [39] A. Ghosh, N. Cheema, C. Oguz, C. Theobalt, and P. Slusallek, "Jl2p: Joint language-to-pose learning for 3d human motion synthesis," in *2021 International Conference on 3D Vision (3DV)*. IEEE, 2021, pp. 181–190.
- [40] M. Zhang, Z. Cai, L. Pan, F. Hong, X. Guo, L. Yang, and Z. Liu, "Motiondiffuse: Text-driven human motion generation with diffusion model," *IEEE transactions on pattern analysis and machine intelligence*, vol. 46, no. 6, pp. 4115–4128, 2024.
- [41] G. Tevet, B. Gordon, A. Hertz, A. H. Bermano, and D. Cohen-Or, "Motionclip: Exposing human motion generation to clip space," in *European Conference on Computer Vision*. Springer, 2022, pp. 358–374.
- [42] M. Zhang, X. Guo, L. Pan, Z. Cai, F. Hong, H. Li, L. Yang, and Z. Liu, "Remodiffuse: Retrieval-augmented motion diffusion model," in *Proceedings of the IEEE/CVF International Conference on Computer Vision*, 2023, pp. 364–373.

[43] Q. Zhang, J. Tao, J. Yang, and Y. Chen, "Diffcollage: Parallel generation of large content with diffusion models," in *Proceedings of the IEEE/CVF Conference on Computer Vision and Pattern Recognition*, 2023, pp. 10188–10198.

[44] S. Lu, L.-H. Chen, A. Zeng, J. Lin, R. Zhang, L. Zhang, and H.-Y. Shum, "Humantomo: Text-aligned whole-body motion generation," in *International Conference on Machine Learning*. PMLR, 2024, pp. 32939–32977.

[45] Y. Wang, Z. Leng, F. W. Li, S.-C. Wu, and X. Liang, "Fg-t2m: Fine-grained text-driven human motion generation via diffusion model," in *Proceedings of the IEEE/CVF International Conference on Computer Vision*, 2023, pp. 22035–22044.

[46] Z. Meng, Y. Xie, X. Peng, Z. Han, and H. Jiang, "Rethinking diffusion for text-driven human motion generation: Redundant representations, evaluation, and masked autoregression," in *Proceedings of the Computer Vision and Pattern Recognition Conference*, 2025, pp. 27859–27871.

[47] C. Guo, Y. Mu, M. G. Javed, S. Wang, and L. Cheng, "Momask: Generative masked modeling of 3d human motions," in *Proceedings of the IEEE/CVF Conference on Computer Vision and Pattern Recognition*, 2024, pp. 1900–1910.

[48] E. Pinyoanuntapong, P. Wang, M. Lee, and C. Chen, "Mmm: Generative masked motion model," in *Proceedings of the IEEE/CVF Conference on Computer Vision and Pattern Recognition*, 2024, pp. 1546–1555.

[49] E. Pinyoanuntapong, M. U. Saleem, P. Wang, M. Lee, S. Das, and C. Chen, "Bamm: Bidirectional autoregressive motion model," in *European Conference on Computer Vision*. Springer, 2024, pp. 172–190.

[50] C. Zhong, L. Hu, Z. Zhang, and S. Xia, "Attt2m: Text-driven human motion generation with multi-perspective attention mechanism," in *Proceedings of the IEEE/CVF International Conference on Computer Vision*, 2023, pp. 509–519.

[51] D. Fu, "Mogo: Rq hierarchical causal transformer for high-quality 3d human motion generation," *arXiv preprint arXiv:2412.07797*, 2024.

[52] M. Liu, S. Yan, Y. Wang, Y. Li, G.-B. Bian, and H. Liu, "Mosa: Motion generation with scalable autoregressive modeling," *arXiv preprint arXiv:2511.01200*, 2025.

[53] C. Guo, X. Zuo, S. Wang, and L. Cheng, "Tm2t: Stochastic and tokenized modeling for the reciprocal generation of 3d human motions and texts," in *European Conference on Computer Vision*. Springer, 2022, pp. 580–597.

[54] Q. Zou, S. Yuan, S. Du, Y. Wang, C. Liu, Y. Xu, J. Chen, and X. Ji, "Parco: Part-coordinating text-to-motion synthesis," in *European Conference on Computer Vision*. Springer, 2024, pp. 126–143.

[55] J. Wei, X. Wang, D. Schuurmans, M. Bosma, F. Xia, E. Chi, Q. V. Le, D. Zhou *et al.*, "Chain-of-thought prompting elicits reasoning in large language models," *Advances in neural information processing systems*, vol. 35, pp. 24824–24837, 2022.

[56] H. Shao, S. Qian, H. Xiao, G. Song, Z. Zong, L. Wang, Y. Liu, and H. Li, "Visual cot: Unleashing chain-of-thought reasoning in multimodal language models," *arXiv e-prints*, pp. arXiv–2403, 2024.

[57] W. Harvey and F. Wood, "Visual chain-of-thought diffusion models," *arXiv preprint arXiv:2303.16187*, 2023.

[58] Z. Chen, Q. Zhou, Y. Shen, Y. Hong, Z. Sun, D. Gutfreund, and C. Gan, "Visual chain-of-thought prompting for knowledge-based visual reasoning," in *Proceedings of the AAAI Conference on Artificial Intelligence*, vol. 38, no. 2, 2024, pp. 1254–1262.

[59] D. Rose, V. Himakunthala, A. Ouyang, R. He, A. Mei, Y. Lu, M. Saxon, C. Sonar, D. Mirza, and W. Y. Wang, "Visual chain of thought: bridging logical gaps with multimodal infillings," *arXiv preprint arXiv:2305.02317*, 2023.

[60] W. Feng, W. Zhu, T.-j. Fu, V. Jampani, A. Akula, X. He, S. Basu, X. E. Wang, and W. Y. Wang, "Layoutgpt: Compositional visual planning and generation with large language models," *Advances in Neural Information Processing Systems*, vol. 36, pp. 18225–18250, 2023.

[61] C. H. Song, J. Wu, C. Washington, B. M. Sadler, W.-L. Chao, and Y. Su, "Llm-planner: Few-shot grounded planning for embodied agents with large language models," in *Proceedings of the IEEE/CVF international conference on computer vision*, 2023, pp. 2998–3009.

[62] D. Srivastava, X. Zhang, H. Wen, C. Wen, and Z. Tu, "Lay-your-scene: Natural scene layout generation with diffusion transformers," *arXiv preprint arXiv:2505.04718*, 2025.

[63] S. Li, S. Petrangeli, Y. Shen, X. Chen, and N. Ramakrishnan, "Llms as layout designers: Enhanced spatial reasoning for content-aware layout generation," *arXiv preprint arXiv:2509.16891*, 2025.

[64] E. Chern, Z. Hu, S. Chern, S. Kou, J. Su, Y. Ma, Z. Deng, and P. Liu, "Thinking with generated images," *arXiv preprint arXiv:2505.22525*, 2025.

[65] Z. Su, P. Xia, H. Guo, Z. Liu, Y. Ma, X. Qu, J. Liu, Y. Li, K. Zeng, Z. Yang *et al.*, "Thinking with images for multimodal reasoning: Foundations, methods, and future frontiers," *arXiv preprint arXiv:2506.23918*, 2025.

[66] J. Copet, F. Kreuk, I. Gat, T. Remez, D. Kant, G. Synnaeve, Y. Adi, and A. Défossez, "Simple and controllable music generation," *Advances in Neural Information Processing Systems*, vol. 36, pp. 47704–47720, 2023.

[67] M. W. Lam, Y. Xing, W. You, J. Wu, Z. Yin, F. Jiang, H. Liu, F. Liu, X. Li, W.-T. Lu *et al.*, "Analyzable chain-of-musical-thought prompting for high-fidelity music generation," *arXiv preprint arXiv:2503.19611*, 2025.

[68] J. Wang, C. Xu, C. Yu, Z. Hu, H. Xie, G. Yu, L. Shang, and S. Wang, "Language model based text-to-audio generation: Anti-causally aligned collaborative residual transformers," in *Proceedings of the 2025 Conference on Empirical Methods in Natural Language Processing*, 2025, pp. 26036–26054.

[69] H. Liu, K. Luo, J. Wang, W. Wang, Q. Chen, Z. Zhao, and W. Xue, "Thinksound: Chain-of-thought reasoning in multimodal llms for audio generation and editing," in *The Thirty-ninth Annual Conference on Neural Information Processing Systems*.

[70] J. Wang, C. Xu, C. Yu, L. Shang, Z. Hu, S. Wang, and L. Bo, "Synchronized video-to-audio generation via mel quantization-continuum decomposition," in *Proceedings of the Computer Vision and Pattern Recognition Conference*, 2025, pp. 3111–3120.

[71] J. Cha and J. Kim, "Cot-pose: Chain-of-thought reasoning for 3d pose generation from abstract prompts," in *Proceedings of the IEEE/CVF International Conference on Computer Vision*, 2025, pp. 4301–4309.

[72] A. Radford, J. W. Kim, C. Hallacy, A. Ramesh, G. Goh, S. Agarwal, G. Sastry, A. Askell, P. Mishkin, J. Clark *et al.*, "Learning transferable visual models from natural language supervision," in *International conference on machine learning*. PMLR, 2021, pp. 8748–8763.

[73] M. Petrovich, M. J. Black, and G. Varol, "Tmr: Text-to-motion retrieval using contrastive 3d human motion synthesis," in *Proceedings of the IEEE/CVF International Conference on Computer Vision*, 2023, pp. 9488–9497.

[74] J. Devlin, M.-W. Chang, K. Lee, and K. Toutanova, "Bert: Pre-training of deep bidirectional transformers for language understanding," in *Proceedings of the 2019 conference of the North American chapter of the association for computational linguistics: human language technologies, volume 1 (long and short papers)*, 2019, pp. 4171–4186.

[75] A. Van Den Oord, O. Vinyals *et al.*, "Neural discrete representation learning," *Advances in neural information processing systems*, vol. 30, 2017.

[76] B. Jiang, X. Chen, W. Liu, J. Yu, G. Yu, and T. Chen, "Motiongpt: Human motion as a foreign language," *Advances in Neural Information Processing Systems*, vol. 36, pp. 20067–20079, 2023.

[77] N. Mahmood, N. Ghorbani, N. F. Troje, G. Pons-Moll, and M. J. Black, "Amass: Archive of motion capture as surface shapes," in *Proceedings of the IEEE/CVF international conference on computer vision*, 2019, pp. 5442–5451.

[78] C. Guo, X. Zuo, S. Wang, S. Zou, Q. Sun, A. Deng, M. Gong, and L. Cheng, "Action2motion: Conditioned generation of 3d human motions," in *Proceedings of the 28th ACM International Conference on Multimedia*, 2020, pp. 2021–2029.

[79] N. Shazeer, "Fast transformer decoding: One write-head is all you need," *arXiv preprint arXiv:1911.02150*, 2019.

APPENDIX

USER STUDY

We conduct rigorous user studies to evaluate both motion quality and semantic alignment. All tests employ pairwise comparisons between our method and six baselines: GT, MDM, MoMask, T2M-GPT, ParCo, and BAMM. For each comparison, we generate 40 motions using identical text prompts from the HumanML3D test set.

Protocol. Participants view two video clips synthesized by different methods and select their preferred one based on two criteria: (1) “Which motion more closely resembles that of a real human?” for motion quality, and (2) “Which motion more aligns with the given text?” for semantic alignment. Before testing, each participant completes a training page with fixed example videos to ensure task familiarity. During testing, attention checks are randomly inserted—displaying the message “Attention: Please select the right motion”—and responses failing these checks are excluded from analysis.

Results. We recruit 38 participants with qualified English proficiency, each receiving 6 GBP compensation (average completion time: 30 minutes). All participants pass the filtering criteria. As shown in Figures 8 and 9, our method consistently outperforms all competitors in both motion naturalness and semantic accuracy. Notably, our approach achieves approximately 40% preference rate even against ground-truth samples, demonstrating competitive human-like motion quality.

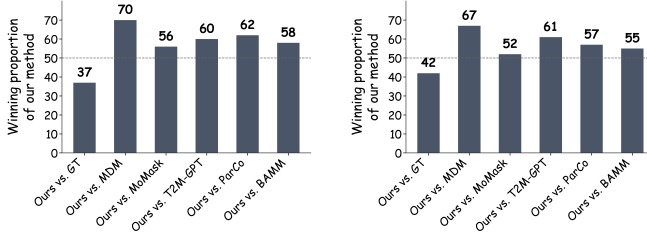


Fig. 8. User study on motion quality. Fig. 9. User study on semantics.

ADDITIONAL ABLATION STUDIES

Impact of Classifier-Free Guidance. We analyze the sensitivity of our LMR framework to the guidance scale s during inference (Figure 10). For the *Continuous Backbone*, performance peaks at $s=5$, achieving FID of **9.937** and Top-1 R-Precision of **0.648**, suggesting that continuous latent spaces require stronger guidance to sharpen the probability density towards the text condition. For the *Discrete Backbone*, the optimal scale is $s=2$ with FID of **0.038** and Top-1 R-Precision of **0.526**. Increasing s beyond this point causes rapid quality degradation, indicating that excessive guidance in discrete spaces leads to probability mass collapse.

Generalizability of Dual-Granularity Strategy. To verify the universality of LMR as a cognitive module, we compare tokenization strategies across both discrete (T2M-GPT) and continuous (MotionStreamer) backbones in Table 8. Our Dual-Granularity strategy employs 1 \times execution tokens for T2M-GPT and 2 \times for MotionStreamer, with reasoning tokens further downsampled by 4 \times relative to execution tokens in both cases.

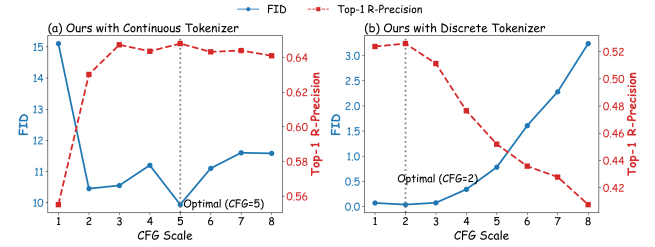


Fig. 10. Impact of Classifier-Free Guidance scale on generation quality and semantic alignment. We evaluate FID and Top-1 R-Precision across varying scales. The continuous MotionStreamer backbone requires a higher guidance scale of 5 for optimal performance. Conversely, the discrete T2M-GPT backbone peaks at a lower scale of 2, suggesting that discrete representations are more sensitive to guidance intensity.

In continuous space, standard baselines exhibit a trade-off where temporal downsampling improves generation but compromises reconstruction; our Dual strategy achieves FID of **9.937** while maintaining semantic consistency. In discrete space, the standard 1 \times scale suffers from poor generation (FID of 0.242) due to semantic sparsity; our Dual strategy achieves an order-of-magnitude improvement to FID of **0.040**, confirming that the reasoning layer effectively bridges the semantic-kinematic gap regardless of backbone architecture. We attribute the varying improvement magnitude to the fundamental properties of latent spaces. The discrete baseline is severely constrained by semantic sparsity, where high-frequency quantization dilutes the reasoning signal, requiring our module to act as a critical stabilizer against structural collapse. Conversely, the continuous framework benefits from the smoothing inductive bias of diffusion, so reasoning latents primarily serve to sharpen semantic alignment rather than rescue the model from contextual sprawl inherent to discrete domains.

TABLE 8
Comparison with different tokenizer strategies in Continuous and Discrete spaces. \mathcal{D} denotes the temporal downsampling rate (e.g., 2 \times implies sequence length $T/2$). ‘Dual’ indicates our proposed dual-granularity strategy.

Method	\mathcal{D}	FID \downarrow	R-Precision \uparrow			MM-Dist \downarrow	Div \rightarrow
			Top-1	Top-2	Top-3		
<i>Continuous Latent Space</i>							
MotionStreamer	2 \times	21.836	0.449	0.606	0.684	18.524	27.008
MotionStreamer	4 \times	11.790	0.631	0.802	0.859	16.081	27.284
Ours	Dual	9.937	0.644	0.812	0.869	15.968	27.373
<i>Discrete Latent Space</i>							
T2M-GPT	1 \times	0.242	0.497	0.684	0.778	3.148	9.914
T2M-GPT	4 \times	0.137	0.482	0.667	0.763	3.359	9.758
Ours	Dual	0.040	0.537	0.721	0.810	2.895	9.668